Int J Adv Manuf Technol (2014) 75:1661–1679
DOI 10.1007/s00170-014-6221-9

ORIGINAL ARTICLE

Five-axis tool path and feed rate optimization based on the cutting force–area quotient potential field

Ke Xu · Kai Tang

Received: 7 December 2013 / Accepted: 31 July 2014 / Published online: 27 August 2014

Abstract Feed rate assignment in five-axis surface machining is constrained by many factors, among which a particularly critical one is the deflection cutting force on the tool: while a larger feed rate increases the machining productivity by shortening the total machining time, it nevertheless inevitably enlarges the deflection cutting force as well, which will cause the tool to be more prone to bending and the machine more prone to vibration, thus adversely degrading the surface finish quality. In this paper, we present a new five-axis tool path generation algorithm that strives to globally maximize feed rate for an arbitrary free-form surface while respecting a given deflection cutting force threshold. The crux of the algorithm is a new concept of the (cutting) force–area quotient function—at any cutter contact point on the surface, the maximal effective material removal rate (with respect to the deflection cutting force threshold) is a continuous function of the feed direction. This function induces a potential field on the surface and based on which an efficient tool path generation algorithm is designed. Preliminary experiments show that substantial reduction in total machining time can often be achieved by the proposed algorithm.

Keywords Five-axis machining · Cutting force · Tool path generation · Effective material removal rate

1 Introduction

Nowadays, free-form surfaces are widely used in aerospace, automobile, mold and die, and other industries. Due to its high degree of freedom and strong capability of global interference avoidance, five-axis milling is a preferred means for machining free-form surface parts, especially at the final finishing stage. At this stage, high machining efficiency and good surface finish are always the key objectives. In terms of machining efficiency, a large material removal rate (MRR) is desired. However, when MRR becomes larger, the cutter will suffer from, among others, a larger cutting force, which will deflect the tool, increase the tool wear rate, and ultimately degrade the surface finish accuracy. In other words, these two desired objectives in general conflict each other.

In order to maintain surface finish quality, the cutter needs to be kept under an acceptable deflection level, wherein the relationship between the deflection force and machining kinematics should be fully investigated. In the past, various cutting force models were proposed. In 1996, Altintas et al. first presented a ball-end milling force model and predicted the force coefficients [1]. Later, Li and Liang [2] extended the model to flat-end 2D pocket milling, and Lee and Lin [3] further established a 3D force model for flat-end milling on sculptured surfaces. Engin and Altintas later extended the work of Lee and Altintaş [1] to a variety of helical end mill profiles by finding the geometric relationship between the tool periphery and the height from the tool tip [4]. While the differential force model proposed in Engin and Altintas [4] is widely used in predicting the instantaneous cutting force, the calculation of cutter contact region was not discussed in Engin and Altintas [4]. Therefore, several methods focusing on the cutter engagement region were developed. Kim et al. used Z-map to determine the cutter contact area in three-axis ball-end milling [5], and they also predicted the mean cutting force using the Z-map method, which is comparatively fast and accurate [6]. Zhu et al. used Z-map to calculate the cutting force in five-axis machining, where the workpiece geometry is updated using a swept envelop [7]. Furthermore, the Octree method is developed in Kim and Ko [8] to more accurately calculate the engagement region. An analytical method was

K. Xu · K. Tang (✉)
The Hong Kong University of Science and Technology, Hong Kong, China
e-mail: mektang@ust.hk

developed by Ozturk and Lazoglu [9] to calculate the precise chip load in three-axis machining. As for force coefficient calibration, most existing methods adopt experimental approaches, such as [10–12], that gave detailed calculation procedures, from which it is well-known that force coefficients vary significantly with both the workpiece material and the cutter profile.

In the realm of improving machining efficiency, past approaches have been mostly following two independent tracks: finding better (i.e., shorter) tool paths and assigning larger (i.e., faster) feed rate. The former is done at the so-called computer-aided manufacturing (CAM) stage where the specific machine tool is not given yet, while the latter is done at the computer numerical controlled (CNC) stage in which the machine tool has been specified. The iso-scallop height tool path generation method was first proposed for both ball-end and flat-end cutter [13,14], where the scallop height formed by adjacent cutter contact curves is kept constant and hence the total path length to cover the whole surface is minimized as compared to other traditional methods. Based on this, some more complicated geometric models were proposed for finding a better solution. Chiou and Lee [15] proposed the concept of machining potential field whose idea is to generate the tool path along the direction that achieves the maximum cutting strip width. Kim and Sarma [16] took the machine performance into consideration and tried to generate tool paths based on the machine's maximum kinematic direction. These optimizations, nevertheless, ignore the mechanics of the machining. In [17], a novel method was presented for the determination of cutter feed direction that tried to minimize the deflection cutting force. Lazoglu et al. [18] presented a force-minimum approach to tool path generation that tried to minimize the average cutting force; the idea is novel but it is limited to three-axis machining only. As for the tool orientation optimization, Ko et al. [19] claimed an inclination angle of 15° would lower the tool wear rate as well as the cutting force. Toh [20] investigated the machining process in inclined hardened steel and suggested a vertical upward orientation that would be better for reducing the cutting force as well as surface roughness. Ozturk et al. [21] fully studied the tool orientation effect in terms of the cutting mechanics and surface quality, recommending different lead and tilt angles for the first cut and the following ones.

After a tool path is generated, at the CNC stage when the specific machine has been determined, maximal feed rate should be sought with all the concerned physical loading constraints respected. Kurt and Bagci [22] gave a thorough review in respect of MRR-based and force-based feed rate scheduling strategies. The latter is arguably more accurate but also more complicated. Erdim et al., Salami et al., and Ko et al. [23–25] developed force-based strategies for the three-axis machining: after the cutting force model of a specific cutter profile is built, the relationship between the force and the feed rate is then established, and finally, the feed rate is regulated under a referenced force value. Feng and Su implemented an integrated method [26] in which the tool path is generated first based on the constant scallop height, and the feed rate is maximized according to the cutting force model. Nevertheless, force-based feed rate scheduling for five-axis machining is scarce in literature, essentially due to the difficulty of modeling the resultant force brought by two additional rotary axes.

To recap, despite many known studies focusing on a variety of cutting force-related topics in multi-axis surface machining, such as the theoretical cutting force model, tool path generation based on minimum cutting force direction at the CAM stage, and feed rate assignment to allow maximum cutting force at the CNC stage, and with many noticeable results, they are mostly restricted to some simplified conditions and, moreover, only applicable to three-axis machining. An optimized tool path computed at the CAM may eventually turn out to be inferior at the CNC stage as the feed rate along the tool path must be restricted by some machine-dependent criteria which are ignored at the CAM stage. Reversely, a best feed rate assignment planned at the CNC stage is only applicable to a fixed (given) tool path, independent of how a tool path is generated in the first place.

In this paper, we present a cutting force-based five-axis surface machining tool path generation algorithm that will take into consideration feed rate scheduling. A cutting force-oriented potential field is first proposed to encapsulate the effective MRR as a function of the feed direction for every point on the part surface. Based on this field, the effective MRR under a threshold deflection cutting force is maximized, and the tool orientation is further adjusted to achieve an even smaller cutting force. The details of the tool path generation are then presented, followed by computer simulation results and comparison data with some leading existing tool path generation algorithms.

2 Preliminary

Before our detailed methodology is introduced, a few terminologies need to be presented first.

Feed rate f: This scalar indicates the tool's relative moving speed on the workpiece.

Feed per tooth f_t: This value shows the tool's movement along feed direction within the time of one tooth rotation.

For a certain tool, if the number of teeth is n, the spindle speed s, the feed rate f, then the feed per tooth is $f_t = \frac{f}{s \cdot n}$. Normally, since n is fixed and s always remains unchanged in a single machining process, f_t is proportional to f.

Tool center: For a ball-end mill cutter, tool center is the center point of the hemisphere of the tool; this point will be regarded as the origin of several coordinate systems to be defined.

Cutter location (CL) curve: When the tool moves along a cutter contact (CC) curve lying on the nominal part surface, the CL curve is the trajectory of the tool tip.

Workpiece coordinate system (WCS): This is a fixed coordinate system defined on the workpiece, formed by its X-, Y-, and Z-axes.

Machining coordinate system (MCS): This coordinate system indicates the tool movement; it originated at the current tool center, consisting of the feed (F), the cross-feed (C), and the surface normal (N) vector; the MCS is a translational form of the local coordinate system.

Tool coordinate system (TCS): This system is a rotated form of MCS with the same origin on the tool center point; any point on the cutter profile can be described by using two angular parameters. The cutting force vectors will be transformed into this coordinate system eventually. The W axis of the system is the tool axis, the U axis is perpendicular to W and lies in the plane formed by the feed (F) and surface normal (N) (i.e., the tangent plane), and V axis is orthogonal to U and W.

Feed angle α: This angle is used to describe the feed direction. The F axis in MCS points toward the feed direction; we project the F axis onto the X–Y plane in WCS, and the angle between the X axis and the projected axis is α.

Lead angle β: This is the angle between the surface normal and the projection of tool axis in the N–F plane.

Tilt angle γ: This is the angle between the tool axis and its projection in the N–F plane.

Raw surface: This is the surface to be processed at the finishing stage, usually a semi-finished surface or a fine casting with a positive offset plus machining error.

Nominal surface: This is the precise theoretical surface, usually mathematically defined, where all the CC points lie. An allowable tolerance is given to gauge the errors between the final machined surface and the nominal surface.

Forward step d: When computing the tool path, the forward step d is the liner distance between any two adjacent CC points, which is controlled by the given chord error e and the normal curvature r along feed direction; more specifically, $d = \sqrt{8er - 4e^2}$ (Fig. 1).

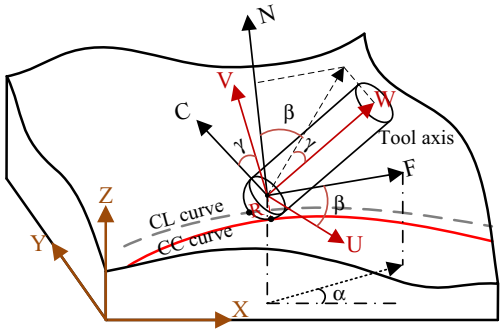

Fig. 1 Definition of coordinate systems, feed angles, and tool orientation angles

3 The force–area quotient potential field

In this section, we introduce the (cutting) force–area quotient potential field by which the effective material removal rate (EMRR) will be determined at each CC point along any feed directions.

3.1 EMRR

First of all, a term named EMRR needs to be defined. In finish machining, the shape error of the machined surface should always be controlled within a tolerance r; in other words, the maximum scallop height h left on the surface should be no more than r. For a nominal surface S, let S' be its offset surface with a positive offset r; the machined surface S_m should then lie in between S and S', as shown in Fig. 2. Therefore, the finish cutting process can be terminated only and only if all the points on S_m are inside the space between S and S'.

EMRR can be viewed as the removal rate of the material in between S and S'. No matter what the raw surface is like, the total machining time only depends on EMRR, which should be maximized as large as possible. Mathematically, instantaneous EMRR can be defined as the product of the feed rate f and the effective cutting area A_p, as given in Eq. (1) and illustrated in Fig. 3.

$$\text{EMRR} = A_p \cdot f \tag{1}$$

3.2 Cutting force–area quotient (FAQ)

As long as the EMRR is enlarged (by increasing the feed rate f) at every CC point, the overall machining time undoubtedly

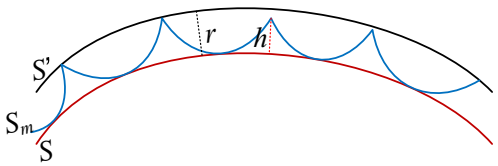

Fig. 2 Relationship between the nominal and machined surfaces

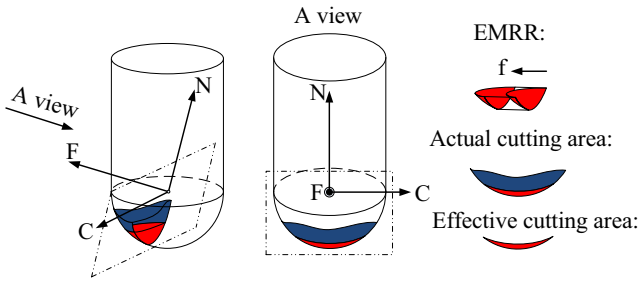

Fig. 3 Definition of EMRR and the effective cutting area

will be reduced. However, as already alluded, when feed rate f increases, the deflection cutting force F_d also gets larger, which may cause the finishing surface quality to deteriorate. So, the relationship between f and F_d should be established first.

In five-axis machining, when the raw and nominal surfaces are given, for every CC point, the kinematics of the tool can be described by four parameters, i.e., the feed rate f, feed angle α, lead angle β, and tilt angle γ. With a fixed chip width, the deflection force at this CC point can also be determined by these four arguments, i.e., F_d can be described as F_d (f, α, β, γ). In this vector field, the lead and tilt angle should be fixed in order to maintain fairness toward different feed directions, so here we initially keep the tool axis coincide with the surface normal at each CC point, i.e., γ and β are set to zero. Thus, the deflection force simplifies to a function of f and α, i.e., F_d (f, α).

It has been a common assumption, based on empirical models, that the deflection force is linearly proportional to the feed rate:

$$F_d(f,\alpha) = k_t(\alpha)\cdot f_t + b(\alpha) = \frac{k_t(\alpha)}{s\cdot n}\cdot f + b(\alpha) \tag{2}$$

where $k_t(\alpha)$ and $b(\alpha)$ are the two linear coefficients, which vary with different feed angle α. Physically, $b(\alpha)$ is the force value under zero feed rate, which is relatively small.

Suppose that the maximally allowable deflection force is given as F_{d0}, which can be determined by the material mechanics of the tool and the workpiece. Then, the largest corresponding feed rate f_0 should be:

$$f_0(\alpha) = \frac{F_{d0} - b(\alpha)}{k_t(\alpha)}\cdot s\cdot n \tag{3}$$

However, $k_t(\alpha)$ and $b(\alpha)$ cannot be directly determined since they are related to the local engagement area and cutting force coefficients. As an alternative, we introduce another method: the feed rate is first fixed to be an arbitrary f'; we then calculate the corresponding force F_d, and the largest feed rate f_0 can be obtained by the following two equations:

$$\frac{F_d}{F_{d0}} = \frac{\frac{k_t(\alpha)}{s\cdot n}\cdot f' + b}{\frac{k_t(\alpha)}{s\cdot n}\cdot f_0 + b} \approx \frac{f'}{f_0} \tag{4}$$

$$f_0 = \frac{F_{d0}}{F_d}\cdot f' \tag{5}$$

In Eq. (5), F_{d0} and f' are constants, and F_d is the deflection force under the fixed feed rate f', which can be denoted as a function of feed angle, i.e., $F_d(\alpha)$. Therefore, f_0 is also a function of α only:

$$f_0(\alpha) = \frac{F_{d0}}{F_d(\alpha)}\cdot f' \tag{6}$$

Also, once the nominal surface is given, due to the changing local curvature, the effective cutting area A_p varies with different feed angles, so A_p can be expressed as $A_p(\alpha)$. Therefore, according to Eq. (1), the maximally allowable EMRR as a function of α is:

$$\mathrm{EMRR}_{\text{max-allowable}}(\alpha) = A_p(\alpha)\cdot f_0(\alpha) = \frac{A_p(\alpha)}{F_d(\alpha)}\cdot F_{d0}\cdot f' \tag{7}$$

where F_{d0} and f' are constants, and we can now find the maximal $\mathrm{EMRR}_{\text{max-allowable}}$ by maximizing $\frac{A_p(\alpha)}{F_d(\alpha)}$, which is a function of the feed angle α. This function is a combination of the effective cutting area and the deflection cutting force, to be called the (cutting) FAQ, that is, $\mathrm{FAQ}(\alpha) = \frac{A_p(\alpha)}{F_d(\alpha)}$. As this function is defined at every point on the part surface, it induces a potential field on the surface, i.e., the FAQ potential field. In particular, for each point on the surface, the feed angle that maximizes its FAQ(α), i.e., $\mathrm{Arg}_\alpha \max(\mathrm{FAQ}(\alpha))$, will be called the *principal direction* and the associated FAQ the principal FAQ.

3.3 Effective cutting area

The effective cutting area A_p will be derived as a function of α. In general, the cutting area is influenced by the surface geometric shape as well as the tool orientation, i.e., the normal curvature k and the lead and tilt angle. However, for ball-end milling, the lead and tilt angle do not affect the effective cutting area as long as the cylindrical part is not engaged with S' (Fig. 4). Meanwhile, normal curvature varies with

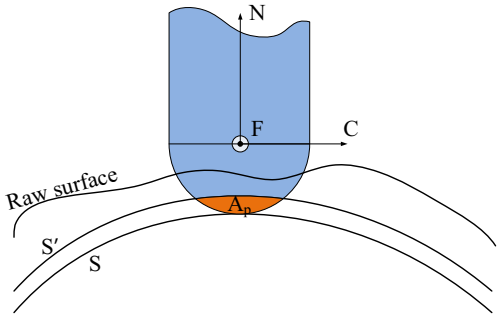

Fig. 4 Effective cutting area

different feed direction, meaning that the effective cutting area is only a function of feed angle α.

The expression of effective cutting area should be derived differently per the sign of the normal curvature, that is, the convex and concave case.

3.3.1 Convex case

In this case, the normal curvature along the cross-feed direction is negative, so that the tool center and the local curvature center are on the opposite sides of the nominal surface. The detailed calculation is given below, as also shown in Fig. 5.

$$\begin{aligned} l &= R + r - h \\ p &= \frac{1}{2}(r + R + l) \\ A_p &= A + B - C = \cos^{-1}\left(\frac{l^2 + R^2 - r^2}{2lR}\right)\cdot R^2 \\ &\quad + \cos^{-1}\left(\frac{l^2 + r^2 - R^2}{2lr}\right)\cdot r^2 - 2\sqrt{p(p-l)(p-r)(p-R)} \end{aligned} \tag{8}$$

3.3.2 Concave case

In this case, the two centers are in a same side of the nominal surface, where the normal curvature is positive, and the calculation is different from the convex case (Fig. 6):

$$\begin{aligned} l &= r + h - R \\ p &= \frac{1}{2}(r + R + l) \\ A_p &= A + B - C = 2\sqrt{p(p-l)(p-r)(p-R)} \\ &\quad + \left(\pi - \cos^{-1}\left(\frac{l^2 + R^2 - r^2}{2lR}\right)\right)\cdot R^2 - \cos^{-1}\left(\frac{l^2 + r^2 - R^2}{2lr}\right)\cdot r^2 \end{aligned} \tag{9}$$

From Eqs. (8) and (9), it is obvious that, at any CC point, A_p is a function of radius r of the normal curvature. As r is a function of the first and second fundamental form which depends on the direction angle α on the tangent plane of the CC point, A_p is a function of α. Figure 7 demonstrates that both the effective cutting area and the normal curvature are sine-shaped functions of the feed angle α, while the two show no phase difference, meaning that the largest normal curvature represents the largest effective cutting area.

3.4 Instantaneous cutting force model

In general, when the tool cuts a workpiece, the generated cutting force is an alternating signal varying with different rotation angle φ. The instantaneous cutting force model is established next to define this dynamic signal.

The tool we used in this paper is a ball-end cutter with a diameter of 12 mm, a helix angle of 30°, and two cutting edges. The maximum allowable axial depth of cut a_p is 20 mm, meaning that the cylinder part of the tool may also get involved in the cutting operation. Based on the above data, for a given nominal surface as well as the raw surface, the instantaneous cutting force can be determined by the following steps.

3.4.1 Step 1: geometric modeling of the ball-end mill

In the TCS, we use the rotation angle φ and the axial height z as the two main parameters to define the transient position of the cutting edge on both the spherical and the cylindrical part.

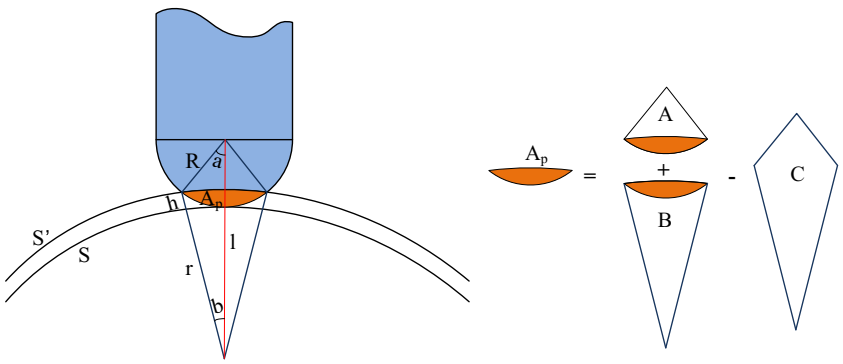

Fig. 5 Calculation of the effective cutting area for the convex case

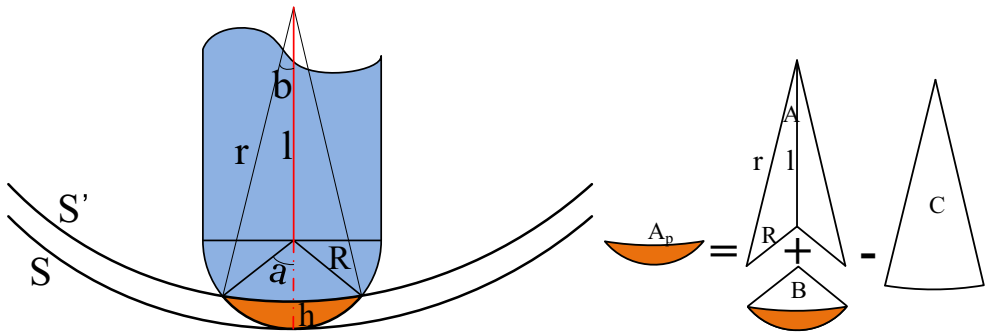

Fig. 6 Calculation of the effective cutting area for the concave case

Referring to Fig. 8, any point on the cutting edge can be defined in TCS as follows.

For the spherical part, where $z<0$:

$$\left(x_p, y_p, z_p\right) = (R\sin(\kappa)\sin(\varphi), R\sin(\kappa)\cos(\varphi), -R\cos(\kappa))$$
$$\kappa = \cos^{-1}(-z/R) \tag{10}$$

where κ is the immersion angle.

For the cylindrical part, where $z\geq 0$:

$$\left(x_p, y_p, z_p\right) = (R\sin(\varphi), R\cos(\varphi), z) \tag{11}$$

Starting from the tool tip with an initial rotation angle φ_0, the rotation angle φ varies with different positions due to the effect of helix angle. Generally, the cutting edge of a ball-end mill is the projection of a helix on the corresponding cylinder, which has a constant helix angle i_0. Their relationship is shown below (Fig. 9):

Therefore, the rotation angle φ is defined as a function of φ_0 and z:

$$\varphi = \varphi_0 - \psi$$
$$\psi = \frac{z+R}{R}\cdot\tan(i_0) \tag{12}$$

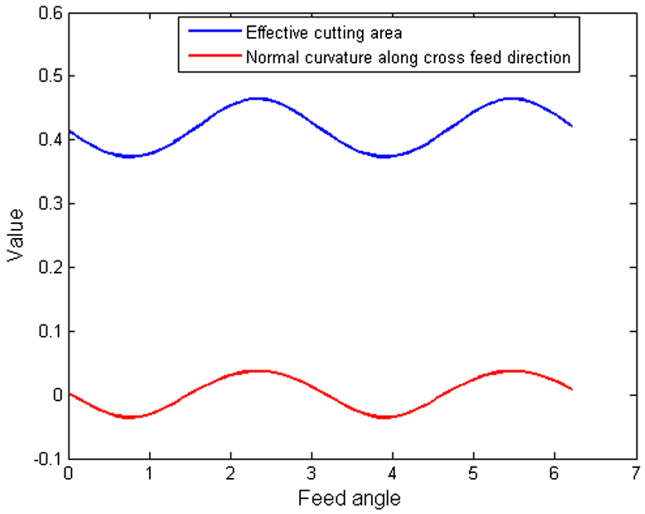

Fig. 7 The effective cutting area and normal curvature vs. feed angle

where ψ is the lag angle which increases along the cutting edge (Fig. 10).

As a result, the point position $\vec{p} = \left(x_p, y_p, z_p\right)$ of the cutting edge can be expressed as follows.

For the spherical part:

$$\left(x_p, y_p, z_p\right) = \begin{pmatrix} R\sin(\kappa)\sin(\varphi_0 - (1-\cos(\kappa))\cdot\tan(i_0)), \\ R\sin(\kappa)\cos(\varphi_0 - (1-\cos(\kappa))\cdot\tan(i_0)), \\ -R\cos(\kappa) \end{pmatrix}$$
$$\kappa = \cos^{-1}(-z/R) \tag{13}$$

For the cylindrical part:

$$\left(x_p, y_p, z_p\right) = \left(R\sin\left(\varphi_0 - \frac{z+R}{R}\cdot\tan(i_0)\right), R\cos\left(\varphi_0 - \frac{z+R}{R}\cdot\tan(i_0)\right), z\right) \tag{14}$$

From Eqs. (13) and (14), the point position on one cutting edge is a function of φ_0 and z, whereas for the other cutting edge, a phase angle π should be added so that the initial rotation angle φ_0' should be $\varphi_0 + \pi$.

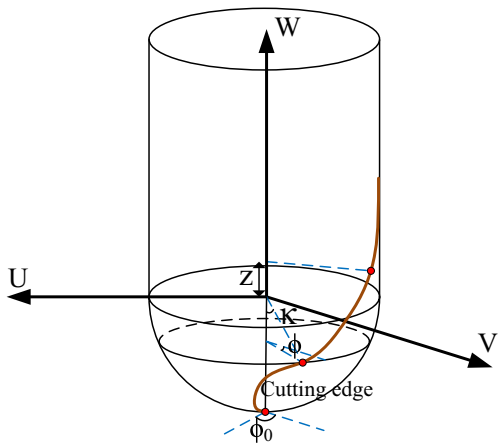

Fig. 8 Point position on the cutting edge

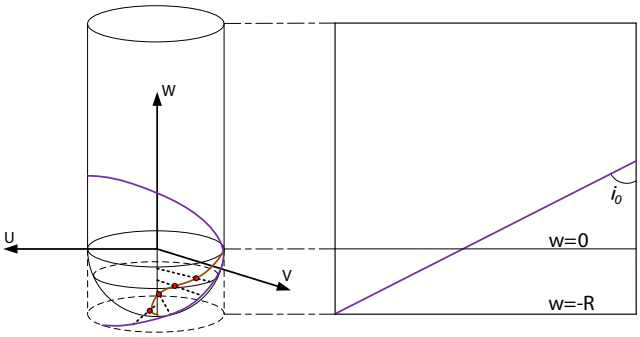

Fig. 9 Construction of a cutting edge

3.4.2 Step 2: modeling of the differential cutting force

The differential tangent (dF_t), radial (dF_r), and subtangent (dF_a) cutting force acting on the point of the cutting edge is first introduced by Lee and Altintas [1] as follows:

$$\begin{aligned} dF_t &= K_{tc}\cdot T(\varphi,\kappa)\cdot db + K_{te}\cdot dz \\ dF_r &= K_{rc}\cdot T(\varphi,\kappa)\cdot db + K_{re}\cdot dz \\ dF_a &= K_{ac}\cdot T(\varphi,\kappa)\cdot db + K_{ae}\cdot dz \end{aligned} \tag{15}$$

where K_{tc}, K_{rc}, and K_{ac} are the shear force coefficients, K_{te}, K_{re}, and K_{ae} the edge coefficients, which can be calibrated by orthogonal experiments, and db and dz the differential chip length and differential projected cutting edge, respectively (Fig. 11). $T(\varphi,\kappa)$ is the chip thickness, which is a product of point position $\vec{p}$ and the feed per tooth vector $\vec{f}_t$ in TCS.

For the spherical part:

$$\begin{aligned} T(\varphi,\kappa) &= \max\left(0, \therefore \vec{f}_t\cdot\vec{p}\right) \\ db &= \frac{dz}{\sin(\kappa)} = Rd\kappa \\ dz &= Rsin(\kappa)d\kappa \end{aligned} \tag{16}$$

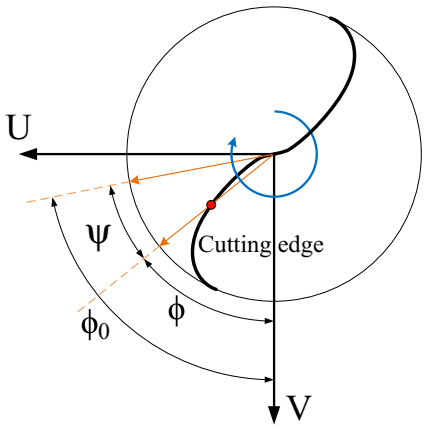

Fig. 10 Definition of lag angle

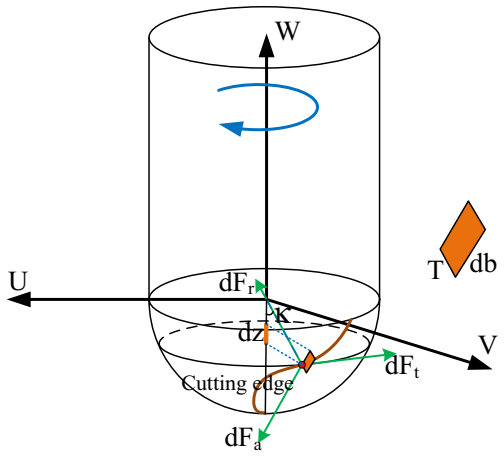

Fig. 11 Differential cutting force exerted on one point of the cutting edge

For the cylindrical part:

$$\begin{aligned} T(\varphi,\kappa) &= \max\left(0, \vec{f}_t\cdot\vec{p}\right) \\ db &= dz \end{aligned} \tag{17}$$

Substitute Eqs. (16) and (17) into Eq. (15), the differential cutting force can be determined by just one differential parameter, $d\kappa$ or dz, respectively, depending on which part of the tool. A transformation matrix helps here to project the cutting force onto TCS, i.e., the u, v, and w direction; thus, the overall deflection force can be calculated by simply adding up all the infinitesimal force elements in a unified coordinate system as follows.

For the spherical part:

$$\begin{bmatrix} dF_u \\ dF_v \\ dF_w \end{bmatrix} = \begin{bmatrix} -\sin(\kappa)\sin(\varphi) & -\cos(\varphi) & -\cos(\kappa)\sin(\varphi) \\ -\sin(\kappa)\cos(\varphi) & \sin(\varphi) & -\cos(\kappa)\cos(\varphi) \\ \cos(\kappa) & 0 & -\sin(\kappa) \end{bmatrix} \begin{bmatrix} dF_r \\ dF_t \\ dF_a \end{bmatrix} \tag{18}$$

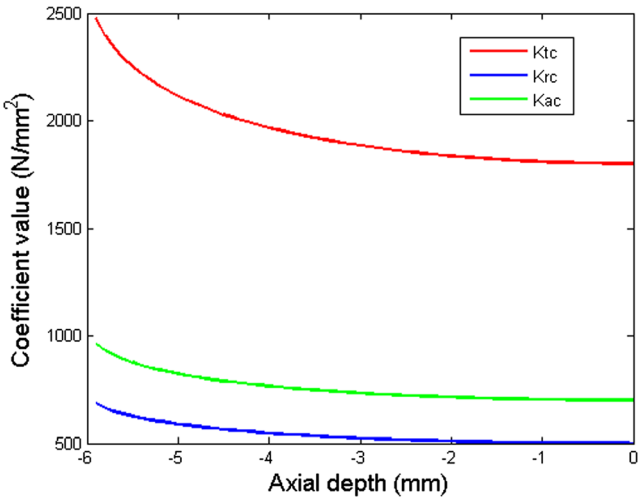

Fig. 12 Cutting force coefficients

For the cylindrical part:

$$\begin{bmatrix} dF_u \\ dF_v \\ dF_w \end{bmatrix} = \begin{bmatrix} -\sin(\varphi) & -\cos(\varphi) & 0 \\ -\cos(\varphi) & \sin(\varphi) & 0 \\ 0 & 0 & -1 \end{bmatrix} \begin{bmatrix} dF_r \\ dF_t \\ dF_a \end{bmatrix} \tag{19}$$

3.4.3 Step 3: determine the engagement region

Once the differential cutting force model is established, the overall deflection force can be calculated by integrating the differential element over the engagement region along the cutting edge, which indicates the actual part of the edge that lies between the raw surface and nominal surface.

In order to determine this region, a complete description of nominal surface as well as raw surface is needed. At the CAM stage, the nominal surface S is usually given in a CAD format (e.g., Bspline), whereas the raw surface S_r remains unknown since it highly depends on the previous machining process. Advanced simulations and digital technologies can be utilized to reconstruct the raw surface into a triangular mesh. Assume the nominal surface as:

$$S(u,v) = (X(u,v), Y(u,v), Z(u,v)) \tag{20}$$

For a given combination of CC point $(x(u,v),y(u,v),z(u,v))$, the feed angle α, the rotation angle φ, and the tool orientation (β, γ), the engagement region due to each cutting edge can be calculated by the following numerical procedure:

1. Start from the tool tip (x_{p0},y_{p0},z_{p0}).
2. Move a differential step Δz along the cutting edge to the next point and transform the point position (x_p,y_p,z_p) from TCS to WCS, i.e., to (x_{pw},y_{pw},z_{pw}).
3. Check whether this point lies in between S and S_r, if so, go back to 2 and continue.
4. Record the critical point (x_{pu},y_{pu},z_{pu}) as the upper boundary, and the engagement region E is part of the cutting edge from the tool tip to the upper boundary.

3.4.4 Step 4: coefficients and integration

To perform the force integration, three shear force coefficients and three edge coefficients are approximated based on Budak and Altintas's work [27]. The constant edge force coefficients are set as K_{te}=25 N/mm, K_{re}=43 N/mm, and K_{ae}=5 N/mm. The shear force coefficients vary with different axial depth z on the spherical part, whereas for the cylindrical part, they are set to be constants (Fig. 12).

With these coefficients determined, we can calculate the total cutting force by the following equation:

$$\begin{pmatrix} F_u \\ F_v \\ F_w \end{pmatrix} = \begin{pmatrix} \int_{(x_{p0},y_{p0},z_{p0})}^{(x_{pu},y_{pu},z_{pu})} dF_u \\ \int_{(x_{p0},y_{p0},z_{p0})}^{(x_{pu},y_{pu},z_{pu})} dF_v \\ \int_{(x_{p0},y_{p0},z_{p0})}^{(x_{pu},y_{pu},z_{pu})} dF_w \end{pmatrix} \tag{21}$$

$$F_d = \sqrt{F_u{}^2 + F_v{}^2}$$

where dF_u, dF_v, and dF_w can be calculated using Eqs. (18) and (19), and F_d is the (magnitude of) instantaneous deflection force.

Figure 13 depicts the simulation result of the instantaneous cutting force for 10 cycles, where the maximum value of F_d is as high as 500 N. Generally speaking, the deflection force signal can be roughly decomposed into a constant none-zero signal F_{dm} and an alternating signal $F_{da}sin(2\varphi)$ with zero mean value:

$$F_d \approx F_{dm} + F_{da}\sin(2\varphi) \tag{22}$$

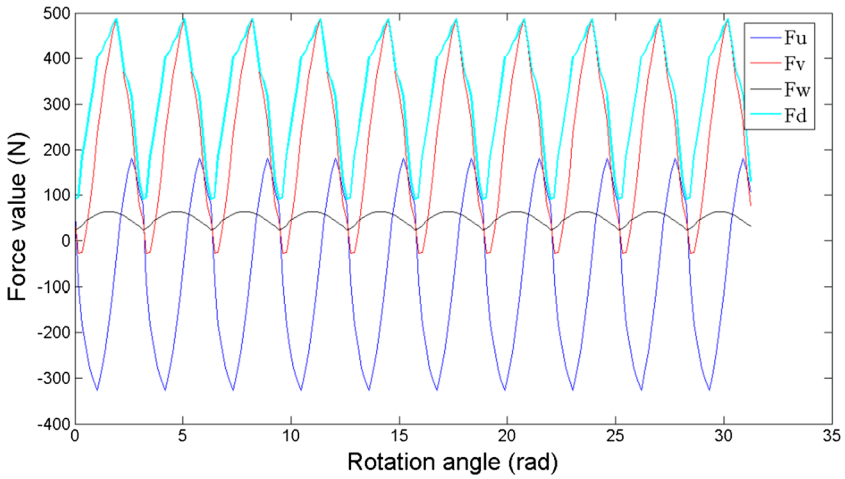

Fig. 13 Instantaneous cutting force signal for 10 cycles

Both signals influence the surface finish quality. If the constant signal is large, which is the mean deflection cutting force, it will dominate the machining error; on the other hand, a large alternating signal F_{da} will cause vibration and deteriorate the surface roughness. Therefore, a natural way to solve this problem is to restrict the summation of the two, i.e., the maximal deflection force during one cycle under a given threshold value.

3.5 Pre-grooving effect

In a typical surface machining process, the workpiece is always cut in a "parallel" fashion: the entire machining is made of a sequence of tool paths each of which has a corresponding (smooth) CC curve. Ignoring the first, when the tool moves along a CC curve, it is only partially submerged between the raw and nominal surface as the previous tool path has already left a "groove" on the surface (see Fig. 14). Because consecutive CC curves are very close to each other on the nominal surface, this so-called pre-grooving effect strongly influences the cutting force and hence cannot be ignored.

In order to calculate the cutting force under this condition, we must consider its effect on the engagement region. As the analytical expression for the groove is virtually impossible to obtain, an alternative approximation scheme should be sought. Let us assume that the previous tool path consists of a series of discrete CC points, i.e.:

$$P_0 = ((x_{01}, y_{01}, z_{01}), (x_{02}, y_{02}, z_{02}) \cdots (x_{0n}, y_{0n}, z_{0n})) \tag{23}$$

Around the neighborhood of each CC point on this CC curve, the groove can be simplified as part of a straight cylindrical surface with the same radius R as the tool nose, and the whole grooved trail generated by this tool path is formed by many small parts of the corresponding cylindrical surfaces, as illustrated below (Fig. 15):

Meanwhile, the current tool path has a non-constant side-step g from the previous one (in order to maintain a constant cusp height on the surface). This side-step g is perpendicular

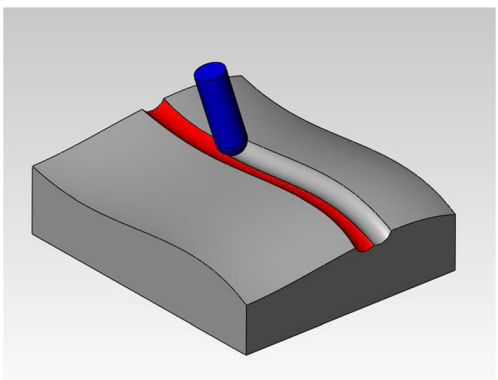

Fig. 14 Grooved trail of the previous tool path

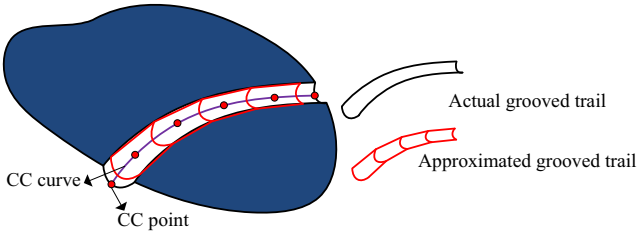

Fig. 15 Approximated groove

to the feed direction and varies at different CC points. For each CC point (x_{0i}, y_{0i}, z_{0i}) on the previous tool path, we can calculate g so that the corresponding CC point (x_{1i}, y_{1i}, z_{1i}) on the current path is determined; these two points provide sufficient information for determining the engagement region, as elaborated in the following steps.

1. For each (x_{1i}, y_{1i}, z_{1i}) on the current tool path, we first calculate the original engagement region E_0 without considering the pre-grooving effect.
2. For the corresponding (x_{0i}, y_{0i}, z_{0i}) on the previous tool path, calculate the tool center location and transform its coordinates into MCS, i.e., $(f_{0ci}, c_{0ci}, n_{0ci})$. The cylindrical surface around this point can be expressed as:

$$S_m = \left\{ (u, v, w) \middle| (v - c_{0ci})^2 + (w - n_{0ci})^2 = R^2, f_{0ci-1} < u < f_{0ci+1} \right\} \tag{24}$$

3. The actual engagement region E must be a subset of E_0. For each point in E_0, transform its coordinates into MCS; if the point lies inside the cylindrical surface S_m (see Fig. 16), remove it.
4. After all the points have been checked and updated in E_0, the remaining region is the actual engagement region with the pre-grooving effect considered, and the corresponding cutting force can be calculated accordingly.

Figure 17 shows an example of the pre-grooving effect on instantaneous deflection force. In the figure, the red curve (with the pre-grooving effect considered) lies below the black one (without considering the pre-grooving effect). In this example, the area below the red curve is only about 60 % of that below the black curve, indicating that the two corresponding mean deflection forces also differ by 40 %, which firmly validates the necessity of consideration of the pre-grooving effect.

4 Tool path generation

In five-axis machining, a tool path is comprised by both a number of smooth CC curves and the corresponding tool orientation along them. Based on the (cutting) force–area

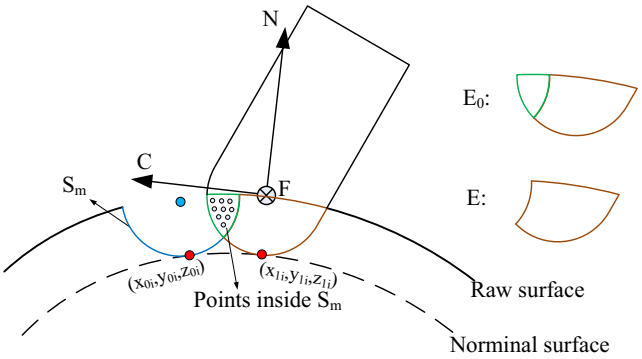

Fig. 16 Determine the engagement region with the pre-grooving effect

quotient potential field model that we have just established, we now present a tool path generation algorithm as well as a feed rate scheduling scheme.

4.1 Generation of CC curves

For a given nominal surface $S(u,v)=(X(u,v),Y(u,v),Z(u,v))$, we divide its square uv domain into an $N\times N$ grid, thus defining a mesh on S. For each node in the mesh, as the domain for the feed angle is from 0° to 360°, the FAQ value is calculated for every δ degree (5 in our current setting), meaning that a total of 72 values will be recorded for each mesh node (Fig. 18). As the tool path has not been generated yet, the pre-grooving effect is not available at this point, and the cutting force model (Section 3.4) is used for calculating these 72 values.

A database D_{FAQ} is built for this field, which contains the discrete nodes' locations as well as the FAQ values in 72 different directions for each node. After the field is built, the CC curves are generated by the following steps.

Step 1 Create an $N\times N$ binary matrix G with all the elements initialized to be "1." This matrix is used to identify the region that has already been covered by the previously already generated tool paths, i.e., the machined area. Another $N\times N$ matrix M is created from D_{FAQ} to store the principal FAQ value for every node in the mesh.

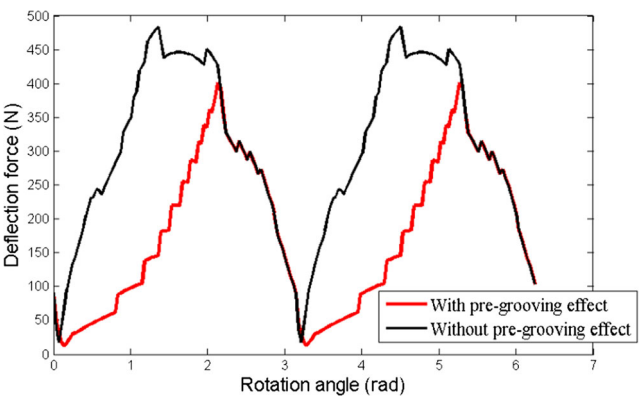

Fig. 17 The deflection force with and without considering the pre-grooving effect

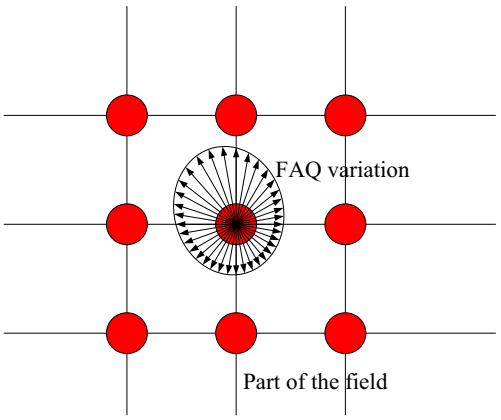

Fig. 18 Discrete force field with varying FAQ

Step 2 For any newly generated CC curve, the matrix G is updated accordingly: for each CC point on the curve, quickly locate the grid square element in G that covers the point and then set all the four nodes of this square element to "0." See Fig. 19 for an example.

Step 3 Update the square matrix M by simply multiplying it with G, so that the mesh nodes already covered by the previous CC curves are removed from further consideration.

$$\begin{bmatrix} m_{11} & \cdots & m_{1n} \\ \vdots & \ddots & \vdots \\ m_{n1} & \cdots & m_{nn} \end{bmatrix}_{new} = \begin{bmatrix} m_{11} & \cdots & m_{1n} \\ \vdots & \ddots & \vdots \\ m_{n1} & \cdots & m_{nn} \end{bmatrix} \times \begin{bmatrix} g_{11} & \cdots & g_{1n} \\ \vdots & \ddots & \vdots \\ g_{n1} & \cdots & g_{nn} \end{bmatrix} = \begin{bmatrix} m_{11}g_{11} & \cdots & m_{1n}g_{1n} \\ \vdots & \ddots & \vdots \\ m_{n1}g_{n1} & \cdots & m_{nn}g_{nn} \end{bmatrix} \tag{25}$$

Step 4 Find a principle node $m_0=(u_0, v_0)$ in the updated M that has the largest difference of FAQ value along different directions, together with its associated

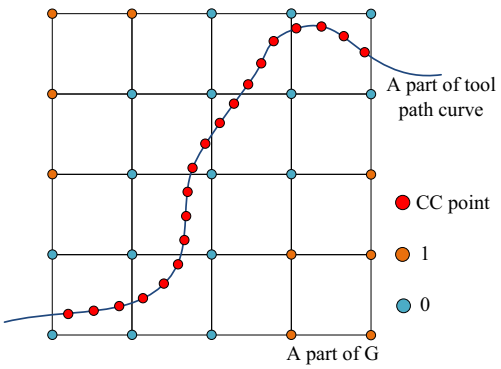

Fig. 19 Updating the G matrix

principal feed angle α_0 found in D_{FAQ}. Start from this initial point along α_0 and advance one forward step d to a new location (u_1, v_1). For the FAQ function at this point, instead of calculating from scratch, it is obtained by interpolating the FAQ values of the four nodes of the square element in uv that covers the point (see Fig. 20). Moreover, since we are only interested in the principal direction at (u_1, v_1), and consider also the fact that FAQ as a function of feed angle changes continuously in uv, the FAQ function at point (u_1, v_1) is computed for only a small range $(\alpha_0-10°, \alpha_0+10°)$. Numerically, the FAQ($\alpha$) in this range is expressed as a degree-four polynomial, with the five points {FAQ($\alpha_0-10°$), FAQ($\alpha_0-5°$), FAQ(α_0), FAQ($\alpha_0+5°$), FAQ($\alpha_0+10°$)} obtained by interpolating the corresponding FAQ values at the four surrounding nodes of (u_1, v_1). The maximum of this polynomial will then be taken as the principal FAQ at (u_1, v_1). The advancement procedure is then repeated at (u_1, v_1), in exactly the same manner as that at (u_0, v_0), and so forth, until either the surface boundary or the machined area (the zero zone in G) is reached. This will conclude the forward part of the CC curve starting at (u_0, v_0).

Step 5 Similar to step 4, except this time we start in the negative principle direction $-\alpha_0$ at (u_0, v_0) (see Fig. 21). The thus generated will be the backward part of the CC curve starting at (u_0, v_0). Combining both the forward and backward part, the resultant CC curve is called a *principal CC curve* which enjoys a unique property: the feed direction at every point on the curve (e.g., the tangent at the point) coincides with the principal feed direction at the point. Physically, this means at every point on the CC curve the tangent direction maximizes the $EMRR_{max\text{-}allowable}$.

Step 6 With the principal CC curve obtained from steps 4 and 5 as the initial curve, the well-known *iso-scallop-height expansion* method [13] is then adopted to generate "parallel" CC curves one-by-one, first to the "left" side of the principal CC curve and then to its "right" side. Since these curves are no longer principal (optimal) ones, a measure will be performed to gauge the quality of the CC curve being expanded: in our current implementation, this measure is the ratio I_C/I_P, where both I_C and I_P are the integrations of the FAQ over the entire CC curve, except that the former is along the tangent direction of the curve, whereas the latter is along the principal direction. If this ratio is less than 80 %, the iso-scallop-height expansion is terminated.

Step 7 Steps 2–6 generate one group of parallel CC curves. We then go back to step 2 to generate another group of parallel CC curves, and so on, until G becomes a zero matrix, which indicates that the entire nominal surface has now been covered.

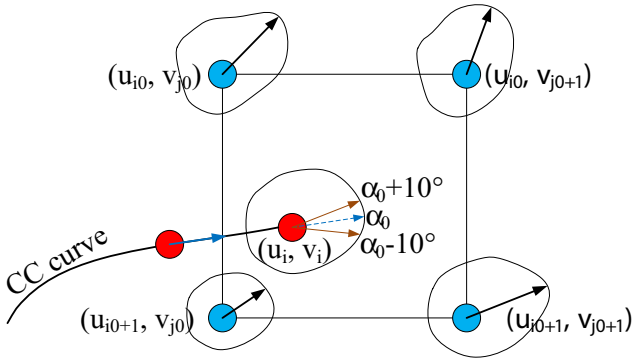

Fig. 20 Feed direction selection

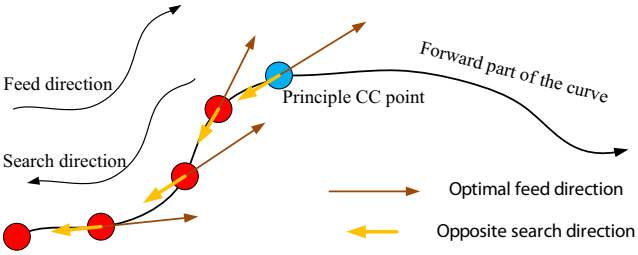

Fig. 21 Backward advancement

4.2 Tool orientation determination

After CC curves are generated, all the CC points and their feed directions are now fixed. We yet must determine the tool orientation at each CC point, i.e., the lead and tilt angle of the tool, which, as we will explain next, should be carefully chosen to consider the pre-grooving effect, so that the FAQ value can be further enlarged.

For ball-end mill, the effective cutting area $A_p(\alpha)$ is only a function of feed angle α, independent of the tool orientation. On the other hand, tool orientation does affect the deflection force. The cutting force model that we have so far established assumes the normal orientation for the tool—the tool axis is the same as the surface is normal. If the lead and/or tilt angle is non-zero, however, the deflection force may alter accordingly. Therefore, the objective is to find better lead and tilt angle for the tool at a given CC point so that the maximum deflection force during one spindle rotation can be reduced, which in turn will further enlarge $EMRR_{max\text{-}allowable}$ (Eq. (7)).

Figure 22a depicts an example of the maximum deflection force during one rotation at a CC point, as a function of the lead and tilt angle, without considering the pre-grooving effect. The maximum deflection force increases slightly when lead angle becomes positive, while a negative tilt angle can drastically increase it, with the minimum occurring at where

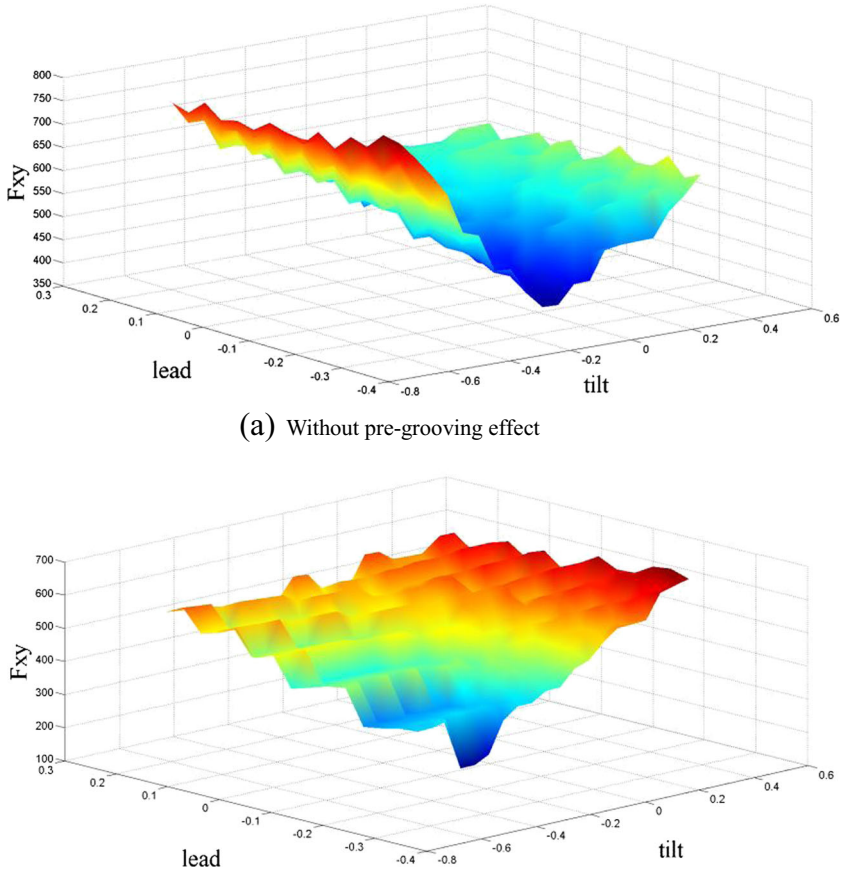

Fig. 22 Maximum deflection force vs. lead and tilt angle. **a** Without pre-grooving effect. **b** With pre-grooving effect

the lead angle is negative and the tilt angle is near zero. Figure 22b shows the same function at the same CC point except this time the pre-grooving effect is considered (where the pre-groove locates in the left side of the current CC curve). The maximum deflection force drops with a decreasing lead angle and rises slightly with an increasing tilt angle, with the minimum occurring when both lead and tilt angle become negative.

From the simulation results shown in Fig. 22, optimal lead and tilt angle can be selected for the tool orientation at each CC point. A relatively lower deflection force can be observed with a negative lead angle, when the axial component of the cutting force is relatively larger (vs. its deflection component) due to the "plunge" motion. It is imperative, however, to emphasize that the determination of tool orientation is affected by many factors, such as global collision avoidance, minimum cutting force requirement, smoothness of the change of tool axis, etc. We nevertheless mainly focus on the maximum deflection force, bearing in mind that the analysis here must be combined with other considerations if the result is to be eventually used in real machining. When only restricted to the maximum deflection force, the lead and tilt angle (β, γ) can be selected differently based on the following three cases.

Case 1 (no pre-grooving effect): The feasible region O_f for (β, γ) is

$$O_{f1} = \left\{ (\beta, \gamma) \middle| -0.5 < \beta < 0.5,\ -0.2 < \gamma < 0.2 \right\} \tag{26}$$

Case 2 (the groove lies in the left side of the feed direction): The feasible region should be

$$O_{f2} = \left\{ (\beta, \gamma) \middle| -0.5 < \beta < 0.5,\ -0.75 < \gamma < -0.25 \right\} \tag{27}$$

Case 3 (the groove lies in the right side of the feed direction): The feasible region is

$$O_{f3} = \left\{ (\beta, \gamma) \middle| -0.5 < \beta < 0.5,\ 0.25 < \gamma < 0.75 \right\} \tag{28}$$

Note that the above selection criteria are specific to the ball-end tool. For other types of tool (e.g., the flat-end), the selection criteria will be different.

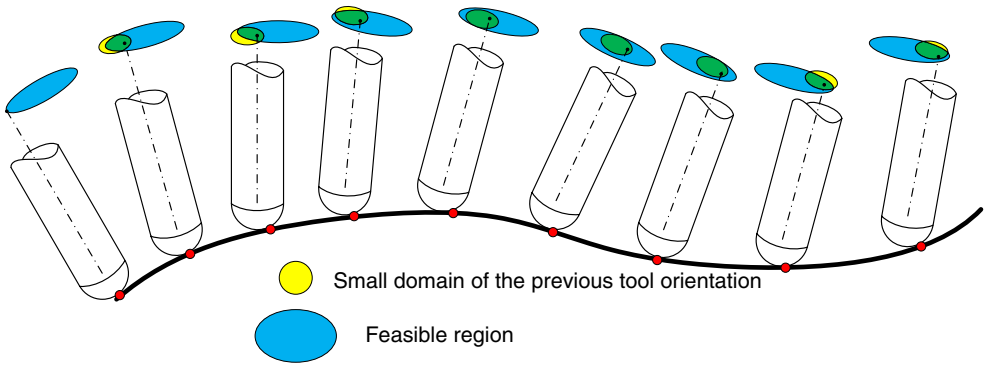

Fig. 23 Incremental algorithm for optimal tool orientation assignment

Once the feasible region for each case is determined, an incremental algorithm is implemented here with an assumption that along one CC curve, the tool orientation as well as the surface normal should change smoothly. The initial tool orientation (β_0,γ_0) is set to be (0, 0) for case 1, (0, −0.5) for case 2, and (0, 0.5) for case 3 on the starting point of any CC curve, and the tool orientation for the next CC point $(\beta_{i+1},\gamma_{i+1})$ is selected within the intersection region O_i consisting of a small domain of the previous one (β_i,γ_i) and the feasible region O_f (see Eq. (29)). In light of this incremental nature, the calculation time for each (β_i,γ_i) is greatly reduced and a smooth variation of tool orientation assures to reduce the jerk (Fig. 23).

$$(\beta_{i+1},\gamma_{i+1})\in O_{ik}=O_{fk}\bigcap\left\{(\beta,\gamma)\middle|(\beta-\beta_i)^2+(\gamma-\gamma_i)^2\le\varepsilon^2\right\},\ k=1,2,3 \tag{29}$$

In Fig. 24, a comparison example is given under a fixed feed rate of 600 mm/min. The CC curve used is a principal CC curve generated in our test example (see Fig. 26), and the lead and tilt angle are selected based on Eqs. (26) and (29) as it is a principal CC curve with no pre-grooving effect. The data convincingly confirms our motivation: as the maximum deflection force of the optimized lead tilt angle is smaller than that of the (0, 0) lead tilt angle (i.e., when the tool axis is the surface normal), the corresponding $\mathrm{EMMR}_{\text{max-allowable}}$ inversely becomes larger (Eq. (7)), thus reducing the total machining time.

4.3 Feed rate scheduling strategy

In deriving Eq. (7), it is assumed that the feed rate is kept constant. In reality, however, at the CNC stage, the feed rate is not constant but always adjusted adaptively to accommodate many physical constraints, e.g., the limit on the angular speed and acceleration. Assuming all these constraints are satisfied, the feed rate for any CC point (in the feed direction) can be decided per Eq. (6) as follows:

$$\max(f_0)=\frac{F_{d0}}{\min(F_d(\beta,\gamma))}\cdot f' \tag{30}$$

where F_{d0} is the given maximum allowable deflection force, $\min(F_d(\beta,\gamma))$ is the minimized maximum deflection force at the CC point (with respect to the feed direction) within its corresponding O_i, and f' is a constant feed rate by which F_d is determined. Note that as F_d is strictly linearly proportional to f', we simply take f' to be 1.

It is necessary to note that the above assignment can only be taken as a reference, and the final feet rate assigned by the CNC controller is usually smaller than this threshold value, as

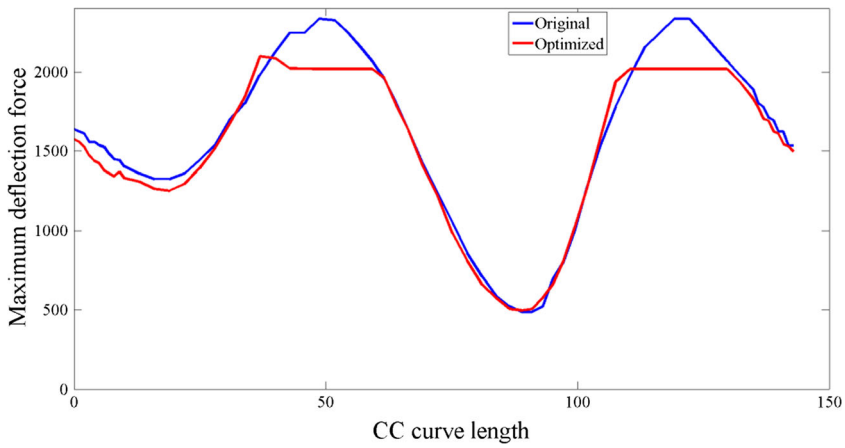

Fig. 24 Comparison of maximum deflection force with different tool orientations along one principle CC curve

all the physical constraints such as the specific machine's kinematics and dynamic capacities must be respected.

5 Experimental results

The presented five-axis tool path generation algorithm based on the proposed cutting force potential field concept has been implemented in MATLAB. The test nominal surface $S(u,v)$ is a parametric free-form surface as shown in Fig. 25 with both valleys and peaks. Through our algorithm in Section 4.1, only one group of iso-scallop-expanded CC curves is generated in this particular example as the ratio I_C/I_P always stays above the critical value 80 %. Tool orientation and feed rate for each CC point are subsequently determined based on the strategies given in Sections 4.2 and 4.3. Figure 26a plots the FAQ field of the surface, which shows a rough trend of the generated tool path shown in Fig. 26b, where the red dot indicates the starting point of the tool path.

To verify the effectiveness of the proposed tool path generation algorithm, a controlled group of tool paths generated by the standard iso-scallop height expansion method is used as the benchmark, as shown in Fig. 27. The tool orientation for this benchmarking group is set to identify with the surface normal.

As an alternative to physical cutting, at least for qualitative verification purpose, a two-phase virtual cutting experiment was conducted on MACHpro (a highly powerful professional post-processing CAM software platform specialized in cutting force simulation). The generated tool paths and feed rate data are transformed into APT files and then imported into MACHpro. We manually set the maximum allowable deflection force F_{d0} to be 1,000 N, the spindle speed to be a constant of 3,000 rpm, and the scallop height to be 0.1 mm. In phase 1, cutting processes for both tool paths are simulated with a constant feed rate value 300 mm/min. Next, in phase 2, feed rate is assigned per CL point to achieve the potential improvement in shorting the machining time. Results are categorized into four data sets, as explained below.

Figures 28, 29, and 30, respectively, demonstrate the corresponding simulation outputs for the benchmarking tool path and the optimized tool paths without and with the adjusted feed rate. For each figure, respectively, the first graph shows the maximal deflection force during the entire machining process, the second one shows the axial cutting force which is perpendicular to the deflection force, and the third and fourth graph depict the chip load and material removal rate, respectively.

For the comparison under a constant feed rate of Fig. 28 vs. Fig. 29, the deflection force exhibits higher value on the

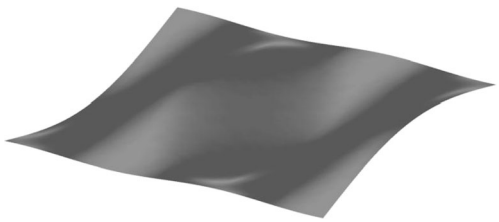

Fig. 25 Nominal surface

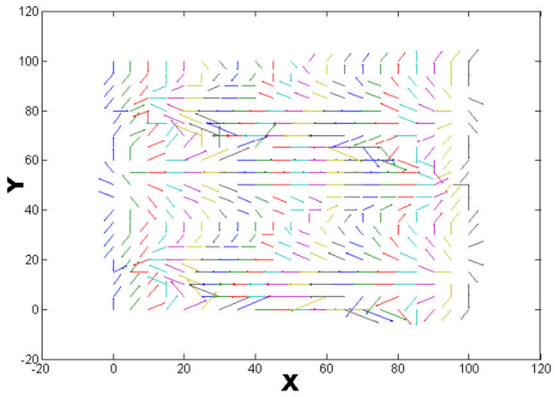

(a) FAQ field of the surface

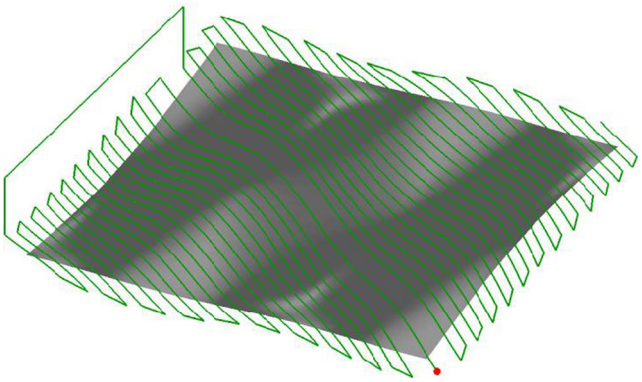

(b) The generated optimal tool path

Fig. 26 FAQ field and the generated CL curves. **a** FAQ field of the surface. **b** The generated optimal tool path

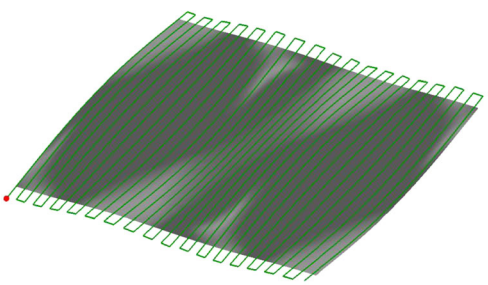

Fig. 27 Benchmarking tool path by the iso-scallop height expansion method

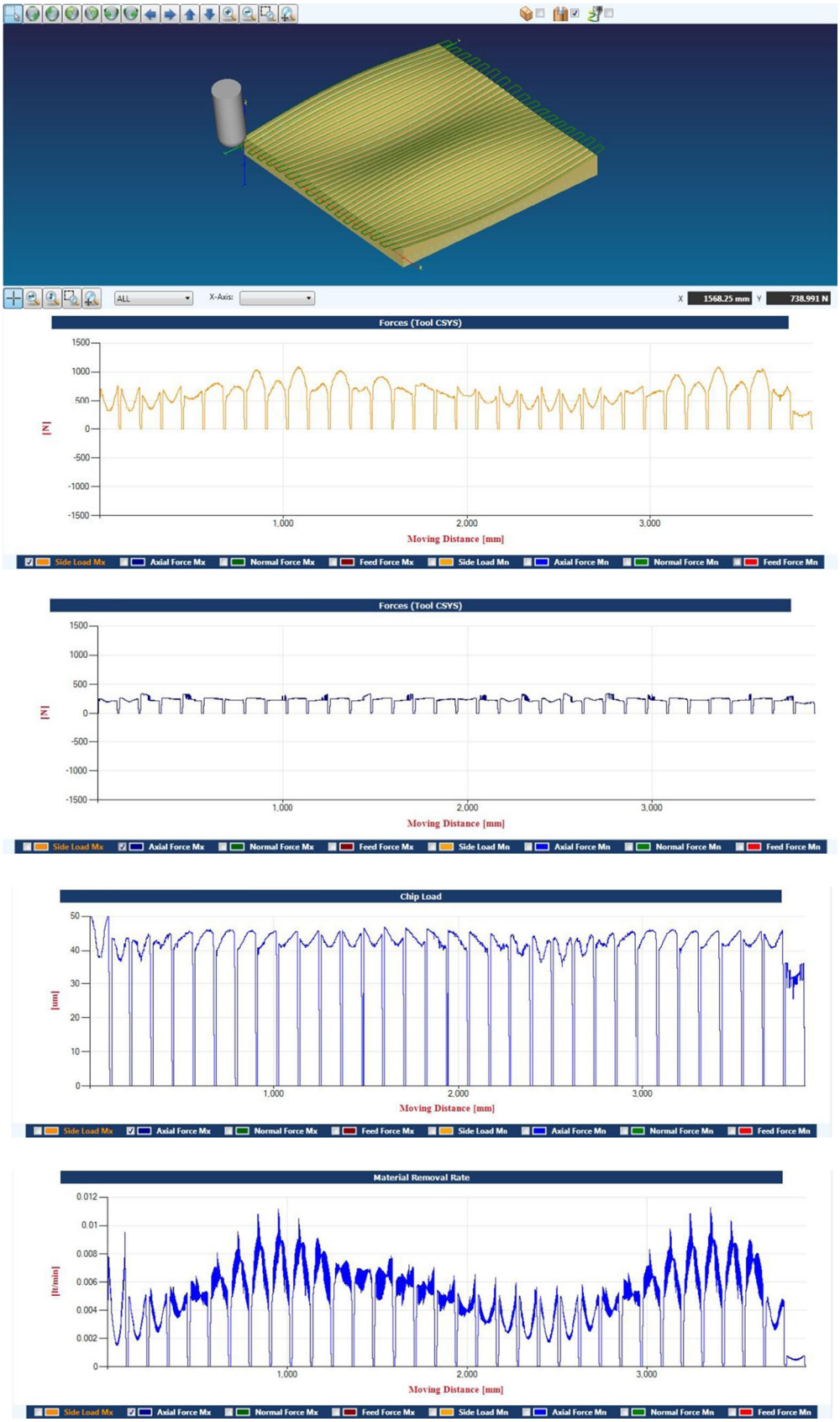

Fig. 28 Experimental result for the benchmarking tool path with constant feed rate

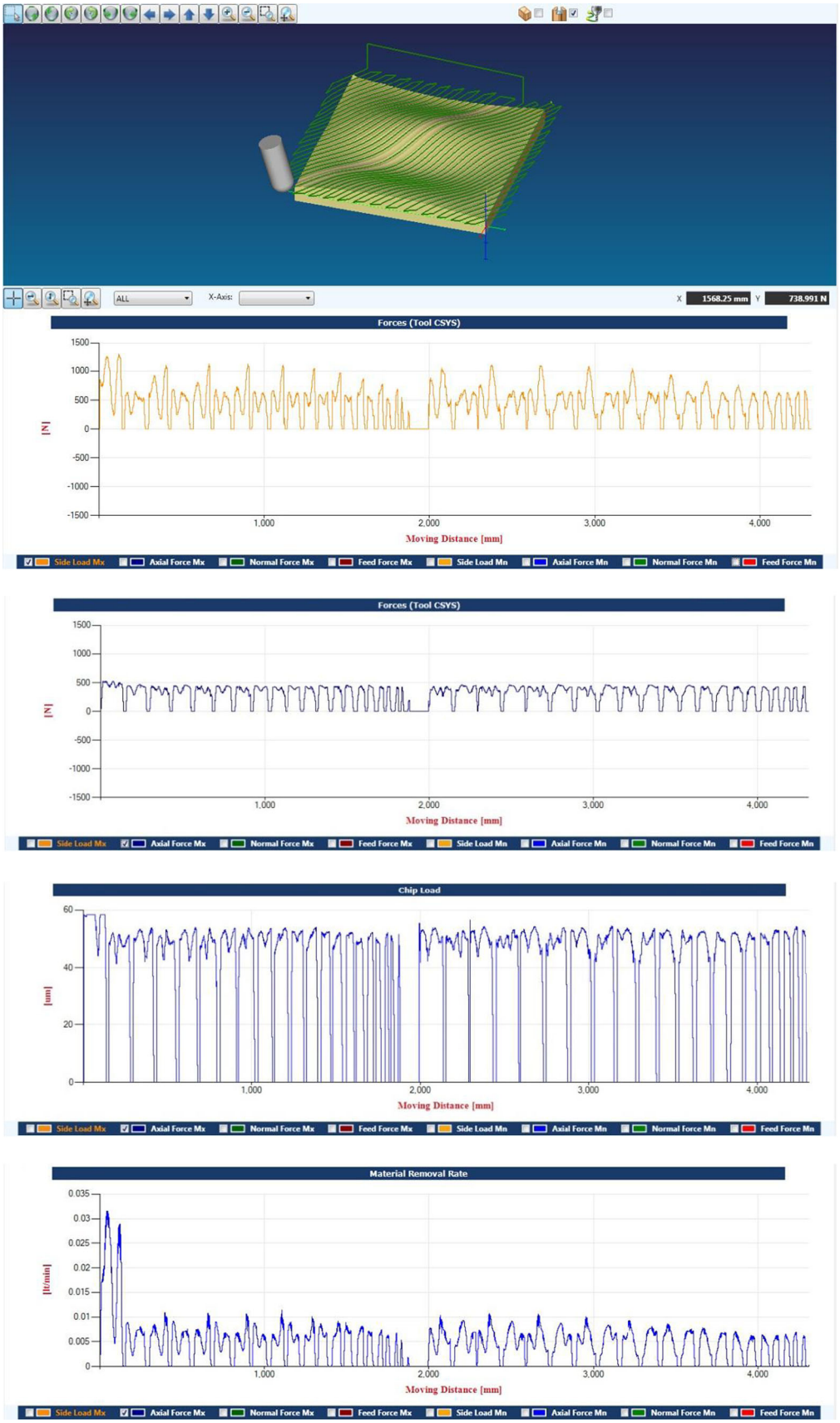

Fig. 29 Experimental result for the optimized tool path with constant feed rate

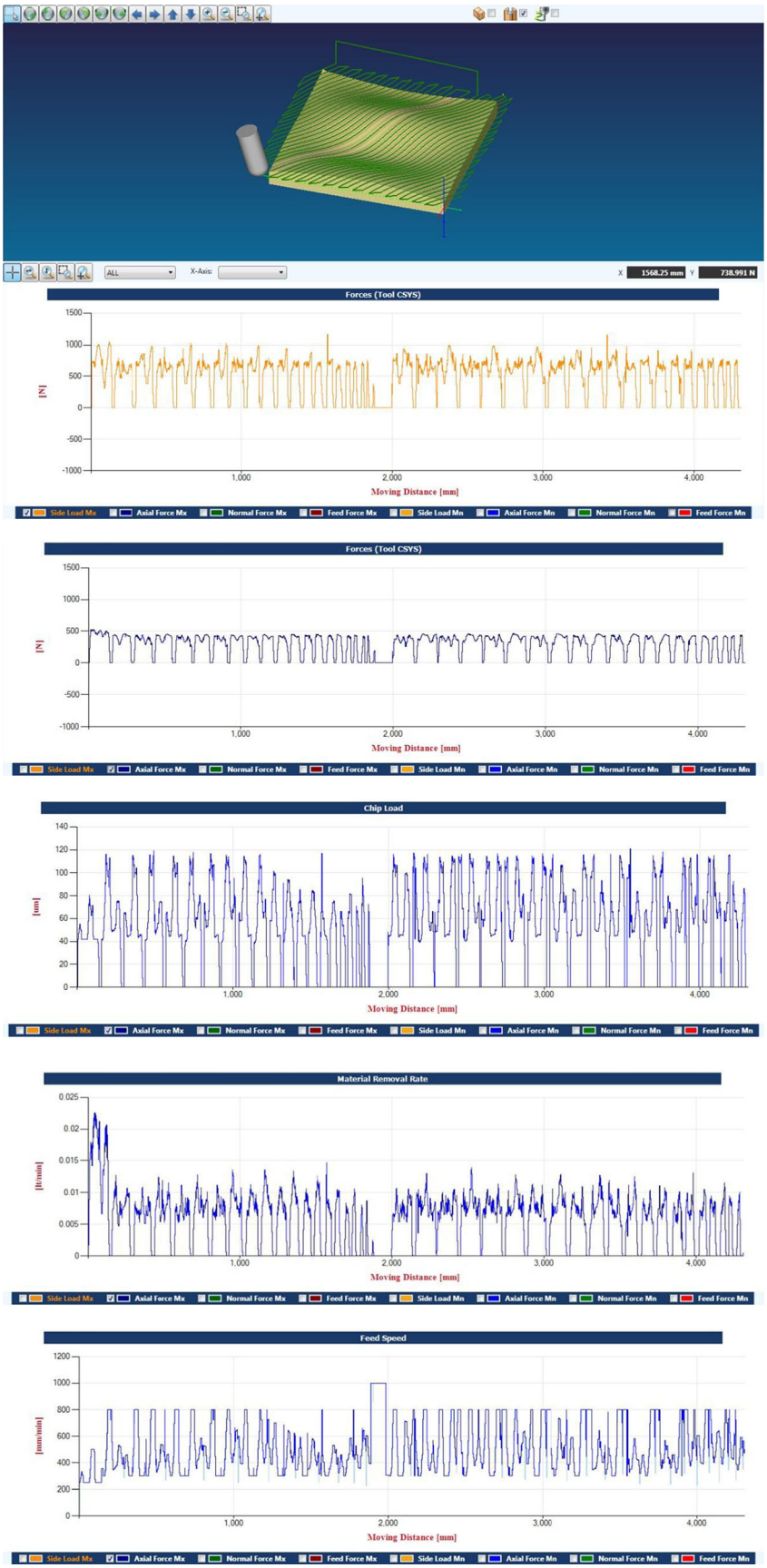

Fig. 30 Experimental result for the optimized tool path with adjusted feed rate

Table 1 Total machining time

Benchmarking tool path	Optimized tool path with constant feed rate	Optimized tool path with adjusted feed rate
776.33 s	738.63 s	583.62 s

benchmarking tool path as more than half of the time it reaches 750 N or above, while on the optimized tool path, it is lower, albeit more fluctuant. Noticeably though, the axial force of the optimized tool path is in general larger than that of the benchmarking one (as a cost of reducing the deflection force), which though is usually of little concern as the tool rigidity in the axial direction is much higher than in the lateral direction. With the chip load being almost the same, the material removal rate for the optimized tool path reaches the highest value (as much as 0.03) along the principle curve and then drops down below 0.01 due to the pre-grooving effect. As the lengths of the two tool paths are almost the same (as expected), and with a same constant feed rate, the optimized tool path achieves little improvement in total machining time against the benchmark (738.63 vs. 776.33 s). However, the lower deflection force of the optimized tool path provides the potential for larger material removal rates after feed rate is rescheduled adaptively, as to be verified in the phase 2 comparison next.

In this comparison (Fig. 30), feed rate is individually adjusted at each CL point under a maximum limit of 800 mm/min to simulate the kinematic capacity of a real machine. Once the CL data together with the scheduled feed rate are input into MACHpro, the built-in machine model will further control the feed rate variation to obey the capacity of machine's acceleration and to reduce the jerk. Result in Fig. 30 shows an enhancement in deflection force with less fluctuation, whose value is well-controlled to approach but stay below the given constraint 1,000 N. The chip load and MRR are also increased due to the improvement of feed rate, resulting in roughly a 25 % reduction in total machining time (Table 1).

6 Conclusion

We have presented a new five-axis tool path generation algorithm for free-form surfaces that takes into consideration the deflection cutting force on the tool when trying to minimize the total machining time. As the deflection cutting force at a CC point depends on many parameters such as the tool orientation, the local geometry of the part surface, the feed direction, and the feed rate, we first conduct a thorough study on their relationships. In addition, to make the mathematical modeling more accurate, we also consider the effect of the adjacent already-cut-groove on the deflection cutting force. Together with the cutting strip width as a function of the feed direction, we then for every CC point define the effective material removal rate as a function of the feed direction and feed rate (with respect to a fixed tool axis). As a result, with respect to a given threshold of deflection cutting force (i.e., the maximally allowable deflection cutting force), for any CC point, every feed direction has a corresponding maximum feed rate. A potential field is then established on the part surface that identifies for every CC point the principal feed direction in which the maximum effective material removal rate can be achieved. Utilizing this potential field, an efficient tool path algorithm is finally designed that strives to adhere to the principal feed direction when the CC curves are determined: at any CC point on a CC curve, the tangent direction should be as close to its principal feed direction as possible. Our preliminary experiments and the comparison results with the popular iso-scallop height tool path generation method show that the proposed method could reduce the total machining time as much as 25 %.

The presented analyses and tool path generation algorithm, however, may produce multiple groups of tool path with some redundant motions such as tool lifting and plunging, which may eventually lower the already-improved machining efficiency in real cutting. A further study is thus needed for a more advanced tool path algorithm toward the objective of minimizing the total machining time considering these additional motions. Moreover, final physical cutting experiments should be conducted to ultimately verify the proposed approach. These will be our next tasks.

References

1. Lee P, Altintaş Y (1996) Prediction of ball-end milling forces from orthogonal cutting data. Int J Mach Tools Manuf 36:1059–1072
2. Li Y, Liang SY (1999) Cutting force analysis in transient state milling processes. Int J Adv Manuf Technol 15:785–790
3. Lee T, Lin Y (2000) A 3D predictive cutting-force model for end milling of parts having sculptured surfaces. Int J Adv Manuf Technol 16:773–783
4. Engin S, Altintas Y (2001) Mechanics and dynamics of general milling cutters. Part I: helical end mills. Int J Mach Tools Manuf 41:2195–2212
5. Kim G, Cho P, Chu C (2000) Cutting force prediction of sculptured surface ball-end milling using Z-map. Int J Mach Tools Manuf 40: 277–291
6. Kim GM, Chu CN (2004) Mean cutting force prediction in ball-end milling using force map method. J Mater Process Technol 146:303–310
7. Zhu R, Kapoor SG, DeVor RE (2001) Mechanistic modeling of the ball end milling process for multi-axis machining of free-form surfaces. J Manuf Sci Eng 123:369–379
8. Kim Y-H, Ko S-L (2006) Improvement of cutting simulation using the octree method. Int J Adv Manuf Technol 28:1152–1160

9. Ozturk B, Lazoglu I (2006) Machining of free-form surfaces. Part I: analytical chip load. Int J Mach Tools Manuf 46:728–735
10. Azeem A, Feng H-Y, Wang L (2004) Simplified and efficient calibration of a mechanistic cutting force model for ball-end milling. Int J Mach Tools Manuf 44:291–298
11. Lamikiz A, LópezdeLacalle L, Sanchez J, Salgado M (2004) Cutting force estimation in sculptured surface milling. Int J Mach Tools Manuf 44:1511–1526
12. Ozturk B, Lazoglu I, Erdim H (2006) Machining of free-form surfaces. Part II: calibration and forces. Int J Mach Tools Manuf 46:736–746
13. Suresh K, Yang D (1994) Constant scallop-height machining of free-form surfaces. J Eng Ind 116:253–259
14. Lo C-C (1999) Efficient cutter-path planning for five-axis surface machining with a flat-end cutter. Comput Aided Des 31:557–566
15. Chiou C-J, Lee Y-S (2002) A machining potential field approach to tool path generation for multi-axis sculptured surface machining. Comput Aided Des 34:357–371
16. Kim T, Sarma SE (2002) Toolpath generation along directions of maximum kinematic performance; a first cut at machine-optimal paths. Comput Aided Des 34:453–468
17. López de Lacalle L, Lamikiz A, Sanchez J, Salgado M (2007) Toolpath selection based on the minimum deflection cutting forces in the programming of complex surfaces milling. Int J Mach Tools Manuf 47:388–400
18. Lazoglu I, Manav C, Murtezaoglu Y (2009) Tool path optimization for free form surface machining. CIRP Ann Manuf Technol 58:101–104
19. Ko T, Kim H, Lee S (2001) Selection of the machining inclination angle in high-speed ball end milling. Int J Adv Manuf Technol 17: 163–170
20. Toh C (2006) Cutter path orientations when high-speed finish milling inclined hardened steel. Int J Adv Manuf Technol 27:473–480
21. Ozturk E, Tunc LT, Budak E (2009) Investigation of lead and tilt angle effects in 5-axis ball-end milling processes. Int J Mach Tools Manuf 49:1053–1062
22. Kurt M, Bagci E (2011) Feedrate optimisation/scheduling on sculptured surface machining: a comprehensive review, applications and future directions. Int J Adv Manuf Technol 55: 1037–1067
23. Erdim H, Lazoglu I, Ozturk B (2006) Feedrate scheduling strategies for free-form surfaces. Int J Mach Tools Manuf 46:747–757
24. Salami R, Sadeghi M, Motakef B (2007) Feed rate optimization for 3-axis ball-end milling of sculptured surfaces. Int J Mach Tools Manuf 47:760–767
25. Ko JH, Yun WS, Cho D-W (2003) Off-line feed rate scheduling using virtual CNC based on an evaluation of cutting performance. Comput Aided Des 35:383–393
26. Feng H-Y, Su N (2000) Integrated tool path and feed rate optimization for the finishing machining of 3D plane surfaces. Int J Mach Tools Manuf 40:1557–1572
27. Budak E, Altintas Y, Armarego E (1996) Prediction of milling force coefficients from orthogonal cutting data. J Eng Ind 118: 216–224